# SUPPLEMENTARY MATERIAL

## Cu-histidinyl catalysts for mild and efficient propargylic alcohol carboxylation with $CO_2$

Yue Liu[‡a,b], Tiansheng Wang[‡a,c], Guilherme Mateus Bousada[a,d], Lionel Salmon[c], Ahmed Subrati[e], Sergio Moya[e], Nathalie Daro[f], Philippe Hapiot[b], Jean-Luc Pozzo[a], Haizhu Yu[g,*], Jean-René Hamon[b,*], Didier Astruc[a,*]

[a] *University of Bordeaux, ISM, UMR CNRS N°5255, 351 Cours de La Libération, 33405 Talence Cedex, France. Email : didier.astruc@u-bordeaux.fr*
[b] *Univ Rennes, CNRS, ISCR (Institut des Sciences Chimiques de Rennes) UMR* 6226, 35000 Rennes, *France. Email : jean-rene.hamon@univ-rennes1.fr*
[c] *LCC, CNRS UPR 8241 & University of Toulouse, 31077 Toulouse Cedex, France*.
[d] *Departamento de Química, Universidade Federal de Viçosa, 36570-900 Viçosa-MG, Brazil.*
[e] *Soft Matter Nanotechnology Lab, CIC biomaGUNE, Paseo Miramón, 182, 20014 Donostia-San Sebastián, Gipuzkoa, Spain*.
[f] *University of Bordeaux, CNRS, Bordeaux INP, ICMCB, UMR 5026, 33600 Pessac, France*
[g] *Department of Chemistry and Center for Atomic Engineering of Advanced Materials, Anhui Province Key Laboratory of Chemistry for Inorganic/Organic Hybrid Functionalized Materials, Anhui University, Hefei, Anhui, 230601 People's Republic of China*. Email : yuhaizhu@ahu.edu.cn
*Corresponding Author.
[‡] Both authors (YL and TW) contributed equally to this work.

**Table of Contents** **pages**

| | |
|---|---|
| $^{1}$H NMR and $^{13}$C NMR spectra and data of the carboxylation products | **S13-19** |

**General information**:
Histidine and $GaBr_3$, 1,1,2,2-tetrachloroethane, 3-methyl-1-pentyn-3-ol, 3,5-dimethyl-1-hexyn-3-ol, 2-phenyl-3-butyn-2-ol and 3-ethyl-1-pentyn-3-ol were purchased from Sigma Aldrich or Fluka. 3,4-dimethyl-1-pentyn-3-ol was purchased from ALFA chemistry, and the other chemicals were supplied by BLD Pharm. All chemicals were commercial without further purification. $^{1}$H and $^{13}$C NMR spectra were recorded at 25 °C with a Bruker AC 300 spectrometer. All the chemical shifts are reported in parts per million ($\delta$, ppm) with reference to $Me_4Si$. Attenuated total reflectance-Fourier transform infrared (ATR-FTIR) spectra were measured on a FT-IR Bruker spectrophotometer. Matrix assisted laser desorption ionization time of flight mass spectrometry (MALDI-TOF MS) spectra were performed by the CESAMO center of the University of Bordeaux, France, on an Autoflex maX TOF mass spectrometer (Bruker Daltonics, Bremen, Germany) equipped with a frequency tripled Nd:YAG laser emitting at 355 nm. Spectra were recorded in the negative-ion mode using the reflectron and with an accelerating voltage of 19 kV. Cyclic Voltammograms (CV) were recorded using Autolab PGSTAT with 3-electrode system at 20 °C, Au (1 mm diameter) working electrode, saturated calomel electrode (SCE) reference electrode, and $NBu_4BF_4$ electrolyte (0.1 M) in DMF. For the High-Resolution Transmission Electron Microscopy (HR-TEM) studies, the copper-gallium nanocatalyst was dispersed in MeOH. Before drop casting on ultrathin (<3 nm) lacey carbon film-coated Cu grids (Ted Pella Inc., USA), dispersion was subjected to soft sonication until it became homogeneous. The grid was left to dry under ambient conditions prior to investigation. HR-TEM experiments were conducted on JEOL JEM-2100F UHR electron microscope (200 kV) equipped with an Energy Dispersive X-ray (EDX) detector (Oxford UltimMax) and two Scanning Transmission Electron Microscopy (STEM) detectors: Bright-Field (BF) and High-Angle Annular Dark-Field (HAADF). For the STEM-EDX studies of the fresh and regenerated catalysts, samples were dispersed in water. Before drop casting on lacey carbon Cu grids (Ted Pella Inc., USA), dispersions were subjected to soft sonication until they became homogeneous. XPS spectra were recorded using the XPS VersaProbe III energy spectrometer. An Al-Kα radiation of 1486 eV was used.

**Preparation of Cu-Ga**:
20 mg CuI (0.1 mmol) and 163 mg histidine (1 mmol) were introduced in 2 mL $CH_3CN$ to form a suspension A, and 10 mg $GaBr_3$ (0.03 mmol) was dissolved in 2 mL DMF to form solution B. A and B were mixed in a well-closed 10-mL Schlenk flask, then 36 μL triethylamine (0.44 mmol) was added to the mixture, and the reaction system was heated to 100 °C for 1 day under $N_2$/vacuum. After the reaction finished, the mixture was cooled down to room temperature (r.t.), followed by washing several times with MeCN and drying under vacuum, 154 mg of the grey-blue solid Cu-Ga was obtained. For $Cu_4$(histidinyl)$_4$GaI.30 His, the compared theoretical mass analyses of C, N, H are given in Table S1, page S5.

**Preparation of Cu-Ga/ZIF-8:**
The nanocatalyst Cu-Ga/ZIF-8 was synthesized by wet impregnation, for which the aqueous solution (15 mg, 2 mL) of Cu-Ga was dropped into the pre-synthesized ZIF-8 powder (100 mg, 8 mL) and vigorously stirred at r.t. for 30 min. The resulting slurry was separated by centrifugation and dried to get the final heterogeneous catalyst Cu-Ga/ZIF-8.

**Procedure for the catalytic cyclic carboxylation of propargylic alcohols**:
In a well-closed 10 mL Schlenk flask, 100 mg of catalyst was taken followed by the addition of 5.0 mmol of propargylic alcohol and 1 mL of triethylamine (TEA). The flask underwent a cycle of vacuum and refilling with carbon dioxide three times before being linked to a $CO_2$ balloon at 1 atm (~0.1MPa). Afterward, the mixture was magnetically stirred at a set temperature, maintaining a stirring rate of 1400 rpm. After the reaction finished, 10 mL of deionized water was added to the reaction mixture, then the solid catalyst was separated by centrifugation (8000 rpm, 5 min) for re-use. The collected homogeneous liquid was washed with ethyl acetate (3 × 10 mL) in a 125 mL separation funnel to keep the organic phase. The mixed organic phase was dried using anhydrous sodium sulphate, and the solvent was removed using a rotary evaporator. The crude residue was analyzed by $^{1}$H NMR, for which 1,1,2,2-tetrachloroethane was employed as the internal standard. The pure compounds were separated by column chromatography utilizing petroleum ether/ethyl acetate as the eluent, with varying ratios ranging from 100:1 to 10:1. Identification of the isolated compounds was carried out using $^{1}$H NMR and $^{13}$C NMR spectra.

## Characterization of the catalysts

### MALDI-TOF-MS

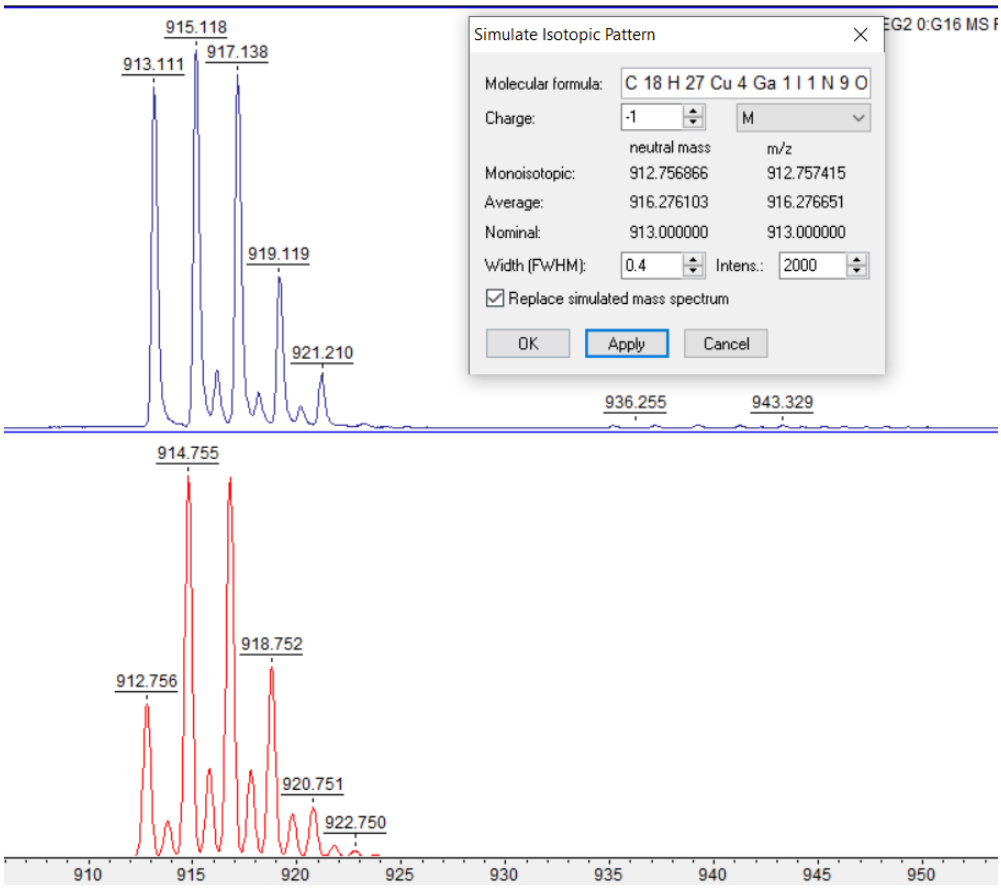


**Figure S1**. Experimental (top, negative mode) and simulated (bottom) isotopic pattern of the peaks corresponding to $[Cu_4(His)_3GaI]^-$.

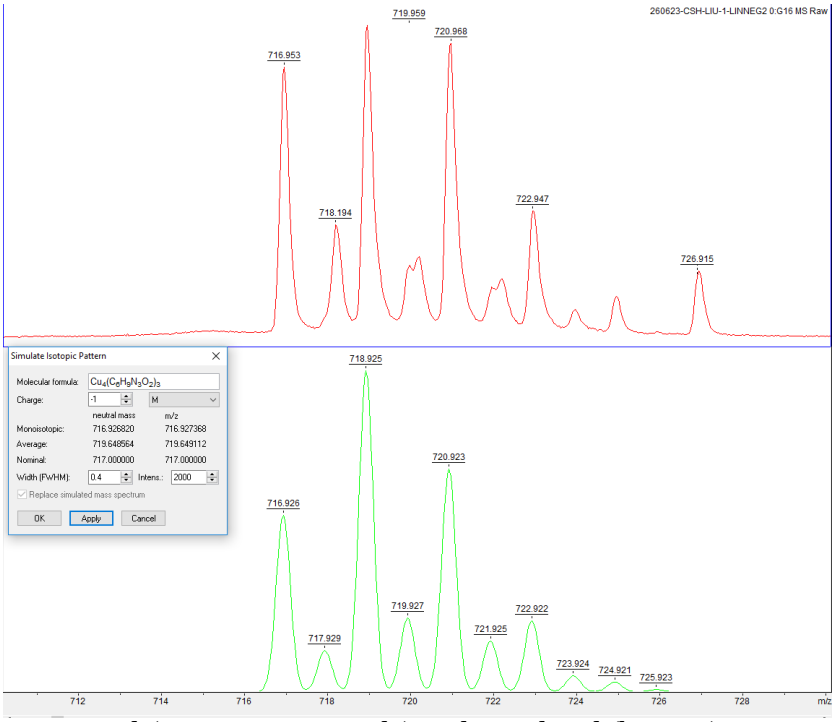


**Figure S2**. Experimental (top, negative mode) and simulated (bottom) isotopic pattern of the peaks corresponding to $[Cu_4(His)_3]^-$.

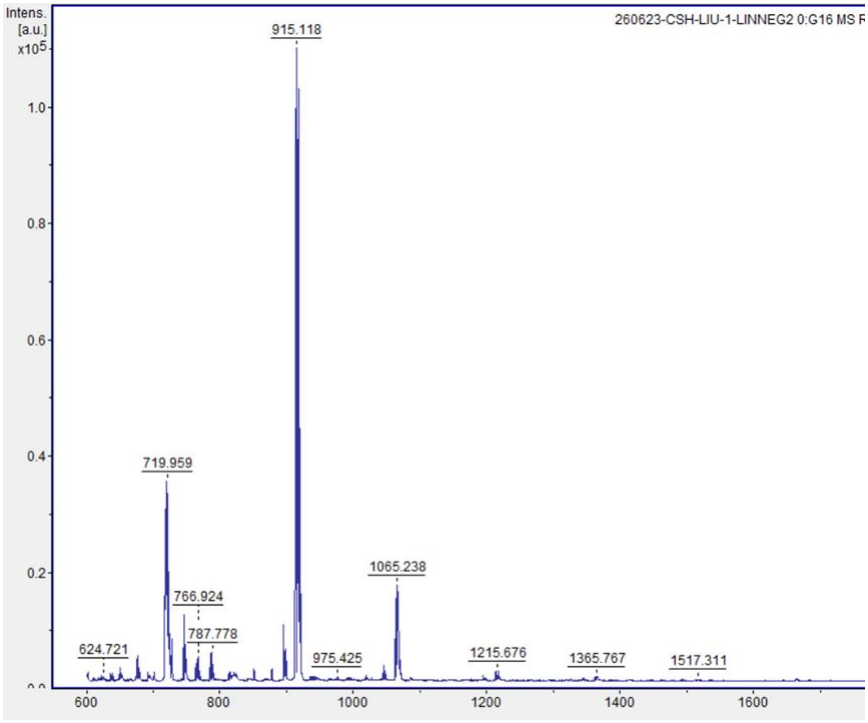


**Figure S3**. Overall MALDI-TOF MS of Cu-Ga (negative mode).

## INFRARED SPECTRA

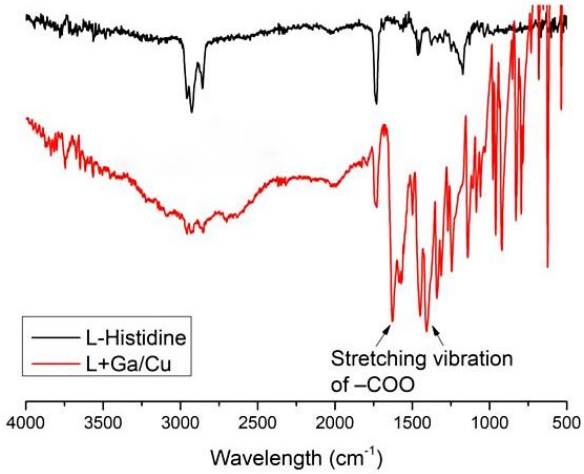


**Figure S4**. Compared IR spectra of histidine (top, black) and Cu-Ga (bottom, red).

## $^{1}$H NMR SPECTRA

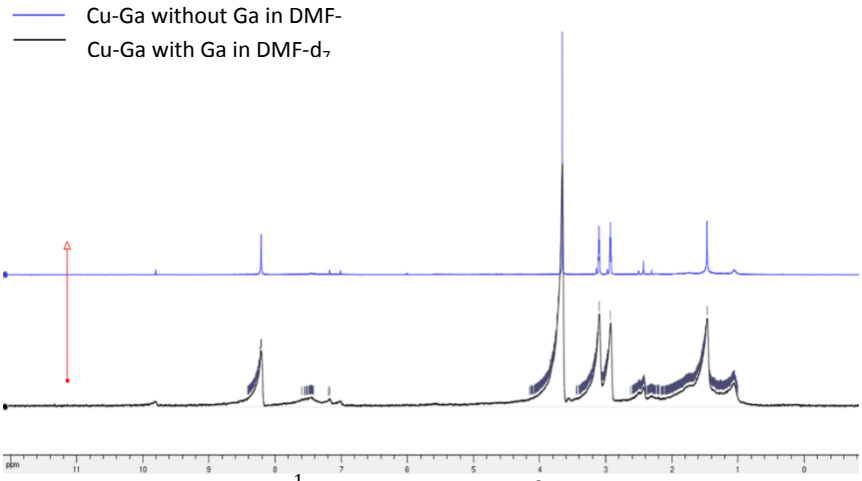


**Figure S5.** Compared $^{1}$H NMR spectra of the catalyst without and with Ga.

Table S1. **CHN elemental analysis of Cu-Ga**

| Sample | Group | Weight (mg) | N (%) | C (%) | H (%) |
|---|---|---|---|---|---|
| Cu-Ga | 1 | 1.7324 | 24.59 | 42.75 | 5.63 |
| | 2 | 1.7337 | 24.75 | 42.89 | 5.71 |
| | Average value | | 24.67 | 42.82 | 5.67 |

Two experimental analyses were conducted (Groups 1 and 2). According to the average of experimental CHN analyses, Cu-Ga contains 42.82% C, 5.67% H and 24.67% N compared to the theoretical analysis of $Cu_4$(histidinyl)$_4$GaI.30 His: 42.82% C, 5.28% H and 24.96% N.

**XPS**

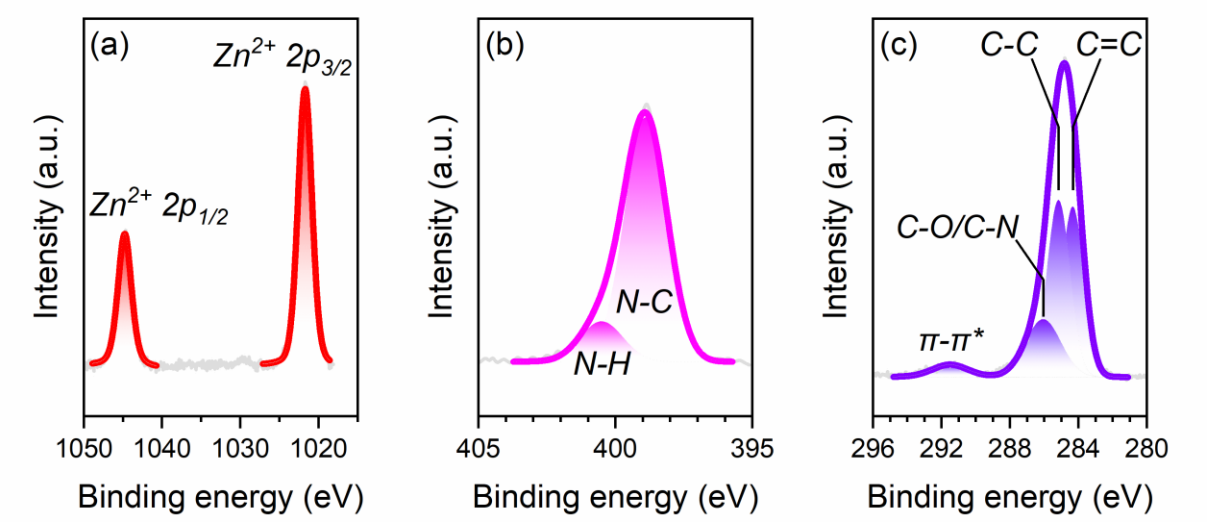


**Figure S6**. XPS analysis of Zn 2p (a), N 1s (b) and C 1s (c) of Cu-Ga/ZIF-8.

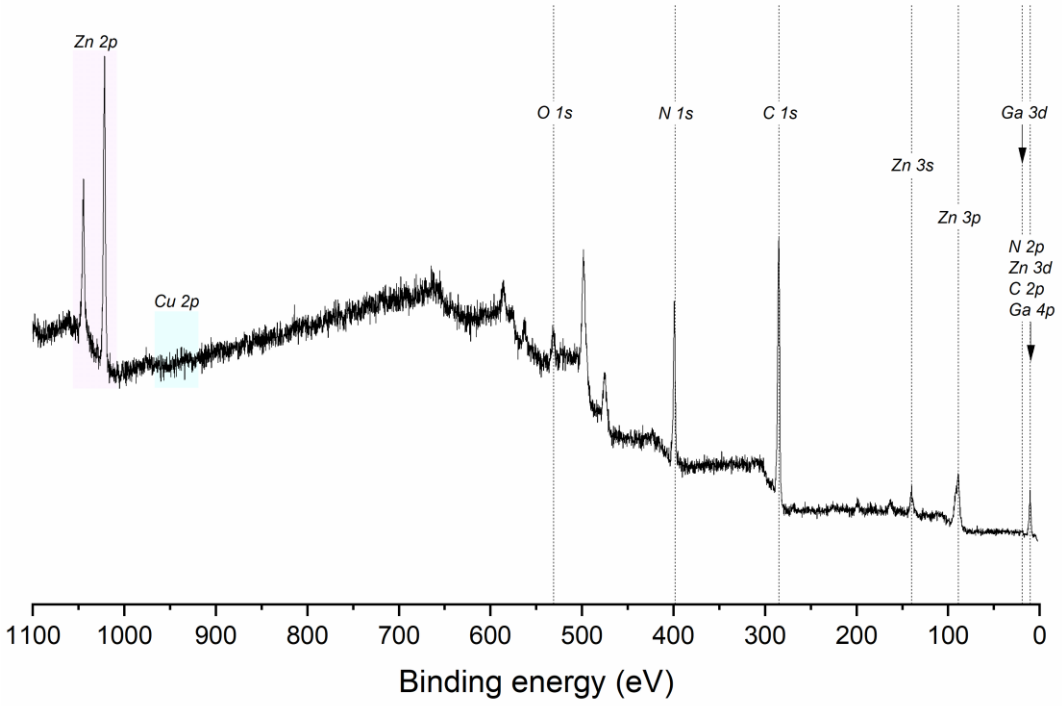


**Figure S7**. Full range XPS survey spectrum of Cu-Ga/ZIF-8. The atomic content of Cu, I, Ga, and O is generally low (Table S2), whereas the signals of Zn, N and C in ZIF-8, the nanocluster support, are intense as can be observed in Figure S6. The low amounts of copper and gallium oxides observed in Figure 2d, are presumably due to small amount of aerobically oxidized species formed between the synthesis and XPS acquisitions through aerobic hydrolysis of CuI and $GaCl_3$. The presence of O is shown by the binding energy at 529.2 eV for Cu–O (coordination), the binding energy at 530.5 eV for Ga–O (coordination), the binding energy at 531.5 eV for C=O (covalent) and the binding energy at 532.8 eV for C–O (covalent).

**XPS**

Table S2. XPS analysis of element contents in Cu-Ga/ZIF-8.

| Element | Component | Binding energy (eV) | Content (at.%) | Total relative content (at.%) |
|---|---|---|---|---|
| Zn | Zn $2p_{3/2}$ | 1021.7 | 76.6 | 4.16 |
| | Zn $2p_{1/2}$ | 1044.8 | 38.3 | |
| C | C=C | 284.3 | 36.8 | 79.53 |
| | C–C | 285.2 | 39.1 | |
| | C–O/C–N | 286.1 | 19.6 | |
| | π-π* | 291.5 | 4.5 | |
| N | N–C | 398.9 | 85.7 | 13.08 |
| | N–H | 400.5 | 14.3 | |
| O | Cu–O | 529.2 | 7.2 | 2.96 |
| | Ga–O | 530.5 | 22.4 | |
| | C=O | 531.5 | 46.6 | |
| | C–O | 532.8 | 23.7 | |
| I | I $3d_{5/2}$ | - | - | 0.00 |
| | I $3d_{3/2}$ | - | - | |
| Cu | $Cu^{+}$ $2p_{3/2}$ | 932.7 | 88.5 | 0.19 |
| | $Cu^{+}$ $2p_{1/2}$ | 952.4 | 44.2 | |
| Ga | $Ga^{+}$ | 18.1 | 80.6 | 0.08 |
| | $Ga^{3+}$ | 19.9 | 19.4 | |

Table S3. **Catalytic activity** of some typical catalysts for cyclization of propargylic alcohols

| Catalyst | Additive/ Solvent | T (℃) | P (atm) | t (h) | TOF[a] ($h^{-1}$) | TON[b] | Refer-ence |
|---|---|---|---|---|---|---|---|
| Ag NPs@SMR | DBU/DMF | 25 | 1 | 10 | 0.91 | - | s1[1] |
| AgOAc | [P66614][DEIm] | 20 | 1 | 30 | 2.97 | - | s2[2] |
| Ag-TCPE | Ph3P/CH3CN | 50 | 5 | 20 | 1.0 | - | s3[3] |
| [Bu4P]3[2,4-OPym-5-Ac] | | 30 | 20 | 5 | 1.82 | - | s4[4] |
| [DBUH][MIM] | - | 60 | 25 | 24 | 0.019 | - | s5[5] |
| Ag@MOF | DBU/DMF | 25 | 1 | 6 | 1.67 | - | s6[6] |
| AgI | KOAc/DMF | 65 | 2 | 12 | 4.17 | 1860 | s7[7] |
| Cu(I)–BPYs | TEA | 50 | 0.5 | 24 | 0.8 | 19.2 | s8[8] |
| Cu-Ga/ZIF-8 | TEA | 50 | 1 | 10 | 8.16 | 96 | This work |

a: TOF (Turnover frequency) was calculated by the mole number of product per mole number of catalyst per hour, and evaluated at the optimal conditions. b: TON (Turnover number) was defined as the mole number of product per mole number of catalyst.

References to Table S3.


(s1) M. Cui, Q. Qian, Z. He, J. Ma, X. Kang, J. Hu, Z. Liu, B. Han, Synthesizing Ag Nanoparticles of Small Size on a Hierarchical Porosity Support for the Carboxylative Cyclization of Propargyl Alcohols with $CO_2$ under Ambient Conditions. Chem Eur J. 45 (2015) 15924-15928. https://doi.org/10.1002/chem.201502479.

(s2) K. Chen, G. Shi, R. Dao, K. Mei, X. Zhou, H. Li, C. Wang, Tuning the Basicity of Ionic Liquids for Efficient Synthesis of Alkylidene Carbonates from $CO_2$ at Atmospheric Pressure. Chem. Commun. 52 (2016) 7830-7837. https://doi.org/10.1039/C6CC02853E.

(s3) Z. Zhou, C. He, L. Yang, Y. Wang, T. Liu, C. Duan, Alkyne Activation by a Porous Silver Coordination Polymer for Heterogeneous Catalysis of Carbon Dioxide Cycloaddition. ACS Catal. 7 (2017)2248-2256. https://doi.org/10.1021/acscatal.6b03404.

(s4) Y. Wu, Y. Zhao, R. Li, B. Yu, Y. Chen, X. Liu, C Wu, X. Luo, Z. Liu, Tetrabutylphosphonium-Based Ionic Liquid Catalyzed $CO_2$ Transformation at Ambient Conditions: A Case of Synthesis of α-Alkylidene Cyclic Carbonates. ACS Catal. 7 (2017) 6251-6255. https://doi.org/10.1021/acscatal.7b01422.

(s5) J. Qiu, Y. Zhao, Z. Li, H. Wang, M. Fan, J. Wang, Efficient Ionic-Liquid-Promoted Chemical Fixation of $CO_2$ into α-Alkylidene Cyclic Carbonates. ChemSusChem. 10 (2017) 1120-1127. https://doi.org/10.1002/cssc.201601129.

(s6) G. Zhang, H. Yang, H. Fei, Unusual Missing Linkers in an Organosulfonate-Based Primitive–Cubic (Pcu)-Type Metal–Organic Framework for $CO_2$ Capture and Conversion under Ambient Conditions. ACS Catal. 8 (2018) 2519–2525. https://doi.org/10.1021/acscatal.7b04189.

(s7) Y. Yuan, Y. Xie, C. Zeng, D. Song, S. Chaemchuen, C. Chen, F. Verpoort, A Simple and Robust AgI/KOAc Catalytic System for the Carboxylative Assembly of Propargyl Alcohols and Carbon Dioxide at Atmospheric Pressure. Catal. Sci. Technol. 7 (2017) 2935–2939. https://doi.org/10.1039/C7CY00696A.

(s8) Z. Shi, J. Jiao, Q. Han, Y. Xiao, L. Huang, M. Li, Synthesis Cu(I)–CN-Based MOF with in-Situ Generated Cyanogroup by Cleavage of Acetonitrile: Highly Efficient for Catalytic Cyclization of Propargylic Alcohols with $CO_2$. Mol. Catal. 496 (2020) 111190. https://doi.org/10.1016/j.mcat.2020.111190.


**XPS and STEM-EDX of the Cu-Ga/ZIF-8 catalyst (Figures S8, S9, and Table S4)**

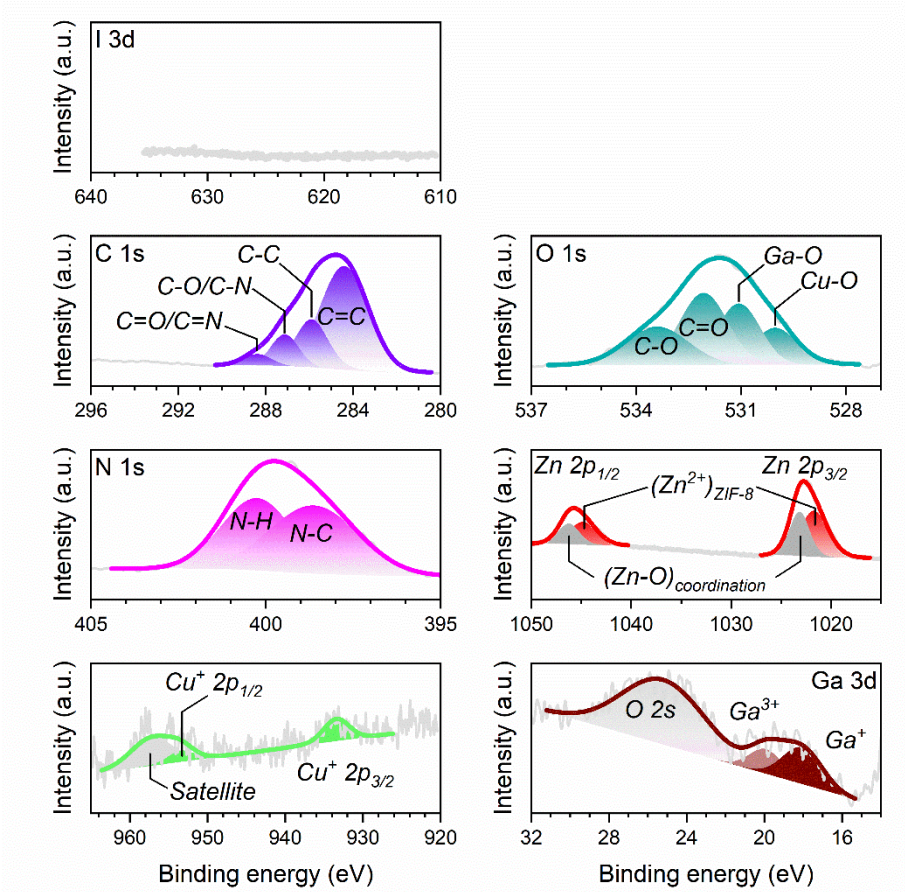


**Figure S8.** XPS analysis of recycled Cu-Ga/ZIF-8. The most notable features exhibited in the recycled catalyst are: (1) The emergence of a Zn-O coordination component that has a larger binding energy (1023.15 eV) [1] than that of the $Zn^{2+}$ found in ZIF-8 (1021.70 eV) [2], and this specific oxygen-coordinated $Zn^{2+}$ is suspected due to the electronegativity of the oxygen present in several oxygen functional groups found in the catalyst. Combined with the STEM-EDX analysis, this interaction can reasonably induce morphological changes in the ZIF-8 structure. (2) The emergence of a satellite peak in the Cu $2p_{1/2}$, which can be attributed to a high coordination state of the $Cu^{+}$ ions. (3) The retention of the Ga-O component, which can be found in the O 1s spectrum [3].

References to Figure S8

[1] S. Gadipelli, Z. Guo. Postsynthesis Annealing of MOF-5 Remarkably Enhances the Framework Structural Stability and $CO_2$ Uptake, Chemistry of Materials 26 (2014) 6333-6338. https://doi.org/10.1021/cm502399q

[2] A. I. A. Soliman, A.-M. A. Abdel-Wahab, H. N. Abdelhamid. Hierarchical porous zeolitic imidazolate frameworks (ZIF-8) and ZnO@N-doped carbon for selective adsorption and photocatalytic degradation of organic pollutants, RSC Advances 12 (2022) 7075-7084. https://doi.org/10.1039/D2RA00503D

[3] S. W. Lee, et al., Unraveling surface structures of gallium promoted transition metal catalysts in $CO_2$ hydrogenation, Nature Communications 14 (2023) 4649. https://doi.org/10.1038/s41467-023-40361-3

Table S4. XPS analysis of element contents in the recycled catalyst Cu-Ga/ZIF-8.

| Element | Component | Binding energy (eV) | Content (%) | Total relative content (%) |
|---|---|---|---|---|
| Zn | $(Zn^{2+})_{ZIF-8}$ Zn $2p_{3/2}$ | 1021.7 | 40.3 | 3.58 |
| | $(Zn\text{-}O)_{coordination}$ Zn $2p_{3/2}$ | 1023.2 | 26.4 | |
| | $(Zn^{2+})_{ZIF-8}$ Zn $2p_{1/2}$ | 1044.8 | 20.1 | |
| | $(Zn\text{-}O)_{coordination}$ Zn $2p_{1/2}$ | 1046.3 | 13.2 | |
| C | C=C | 284.4 | 62.8 | 73.86 |
| | C–C | 285.9 | 21.9 | |
| | C–O/C–N | 287.1 | 11.2 | |
| | C=O/C=N | 288.4 | 4.2 | |
| N | N–C | 398.6 | 54.3 | 14.53 |
| | N–H | 400.2 | 45.7 | |
| O | Cu–O | 530.0 | 17.8 | 7.57 |
| | Ga–O | 531.1 | 25.3 | |
| | C=O | 532.1 | 33.7 | |
| | C–O | 533.4 | 23.2 | |
| I | I $3d_{5/2}$ | - | - | 0.00 |
| | I $3d_{3/2}$ | - | - | |
| Cu | $Cu^{+}$ $2p_{3/2}$ | 933.4 | 28.3 | 0.17 |
| | $Cu^{+}$ $2p_{1/2}$ | 953.4 | 14.2 | |
| | Satellite | 957.2 | 57.5 | |
| Ga | $Ga^{+}$ | 18.0 | 63.3 | 0.28 |
| | $Ga^{3+}$ | 19.9 | 36.7 | |

**STEM-EDX, BF STEM, HAADF STEM of Cu-Ga/ZIF-8**

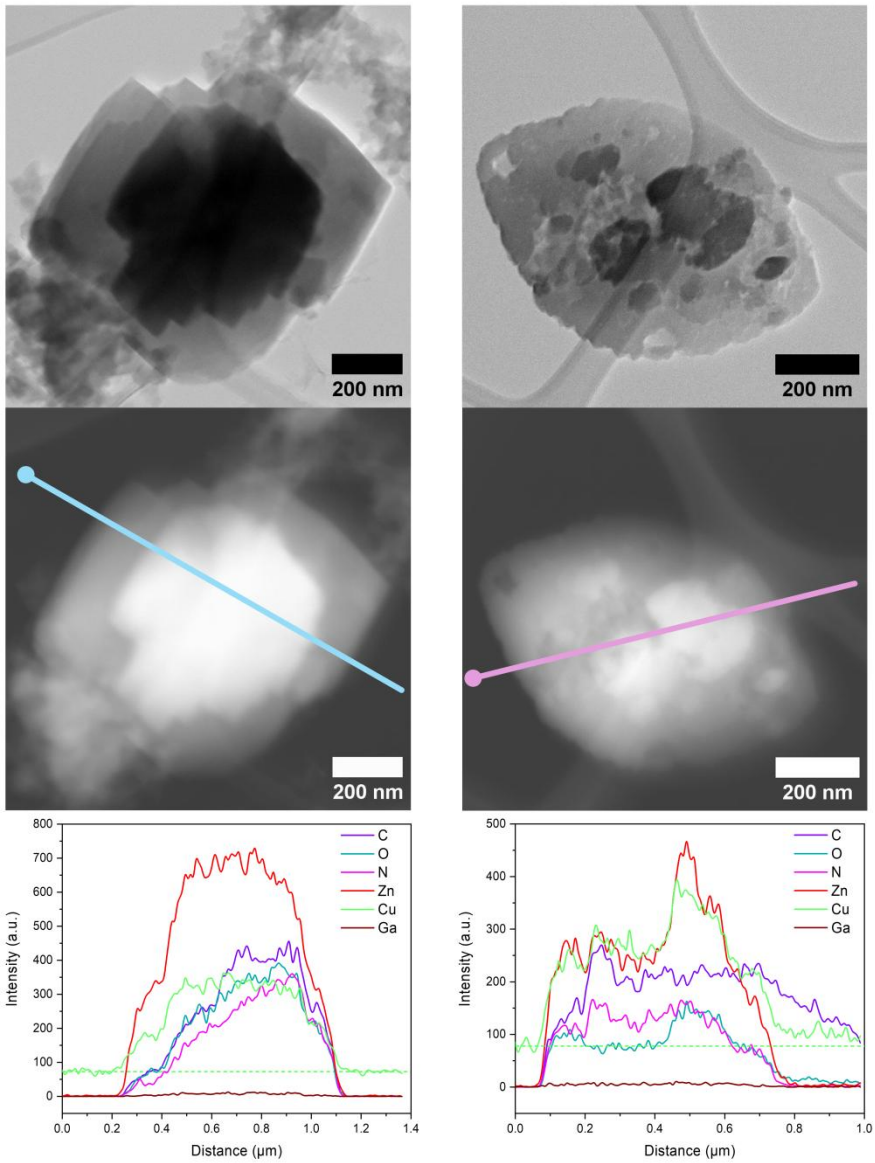


Figure S9. STEM-EDX of fresh (left) and recycled (right) Cu-Ga/ZIF-8. From top to bottom: BF STEM image, HAADF STEM image, and element profile of EDX line scan. Lines in the HAADF STEM images are the EDX line scans with the round heads indicating origins of the line scan profiles. The green dashed line is the background Cu signal. Notice how the distributions of Zn and Cu vary discernibly between the fresh and regenerated Cu-Ga/ZIF-8. Zn and Cu profiles are distinct in both samples. The Cu signals in both samples provide plausible evidence of retention of Cu in catalyst, which is supported by XPS analysis. In the fresh catalyst, the Zn distribution seems to be homogeneous throughout the catalyst particle, whereas in the regenerated catalyst it is inhomogeneous and agglomerated. This can be due to deterioration of lattice structure induced by strong interactions involving lattice Zn(II) of ZIF-8 during reaction cycles, which is supported by XPS analysis. This deterioration renders ZIF-8 particles with limited/disturbed/worsening porosity, which is vital for the overall catalytic process.

**Proposed catalytic mechanism**

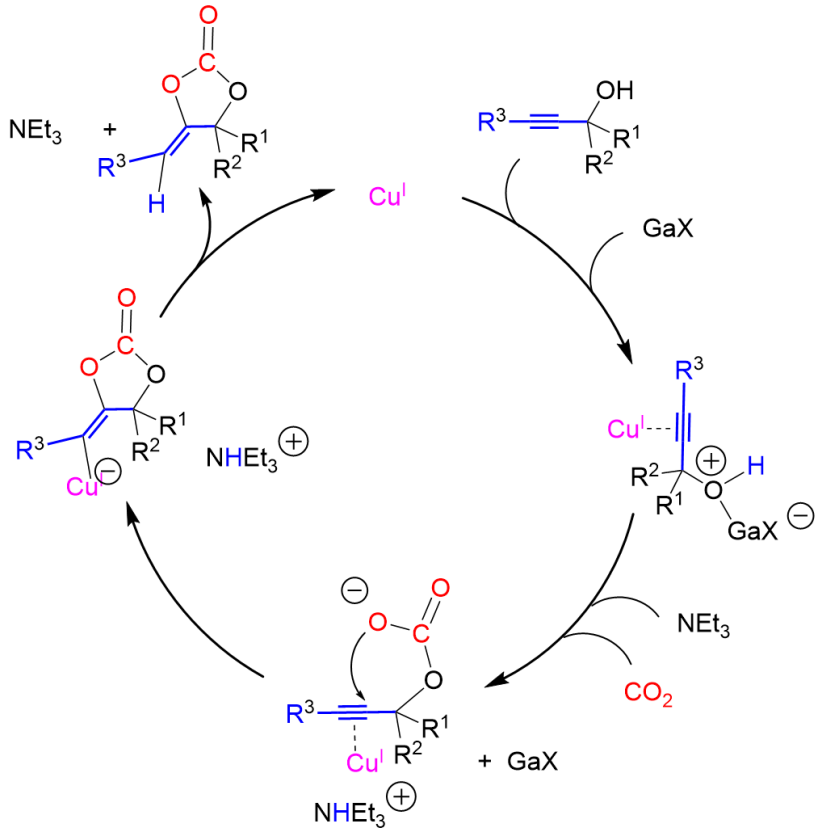


Scheme S1. Proposed mechanism of propargylic alcohol carboxylic cyclization catalyzed by Cu-Ga. With ZIF-8, a Lewis-acidic $Zn^{II}$ center of ZIF-8 is supposed to activate the oxygen atom of propargylic acid in the same way as $Ga^{I}$.

# $^{1}$H NMR and $^{13}$C NMR spectra and data of the carboxylation products

## 4,4-dimethyl-5-methylene-1,3-dioxolan-2-one (2a)

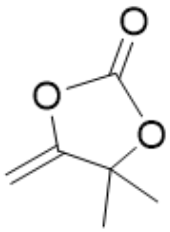

2a

$^{1}$H NMR (300 MHz, $CDCl_3$) δ = 4.68 (d, *J* = 3.9 Hz, 1H), 4.28 (d, *J* = 3.9 Hz, 1H), 1.54 (s, 6H).

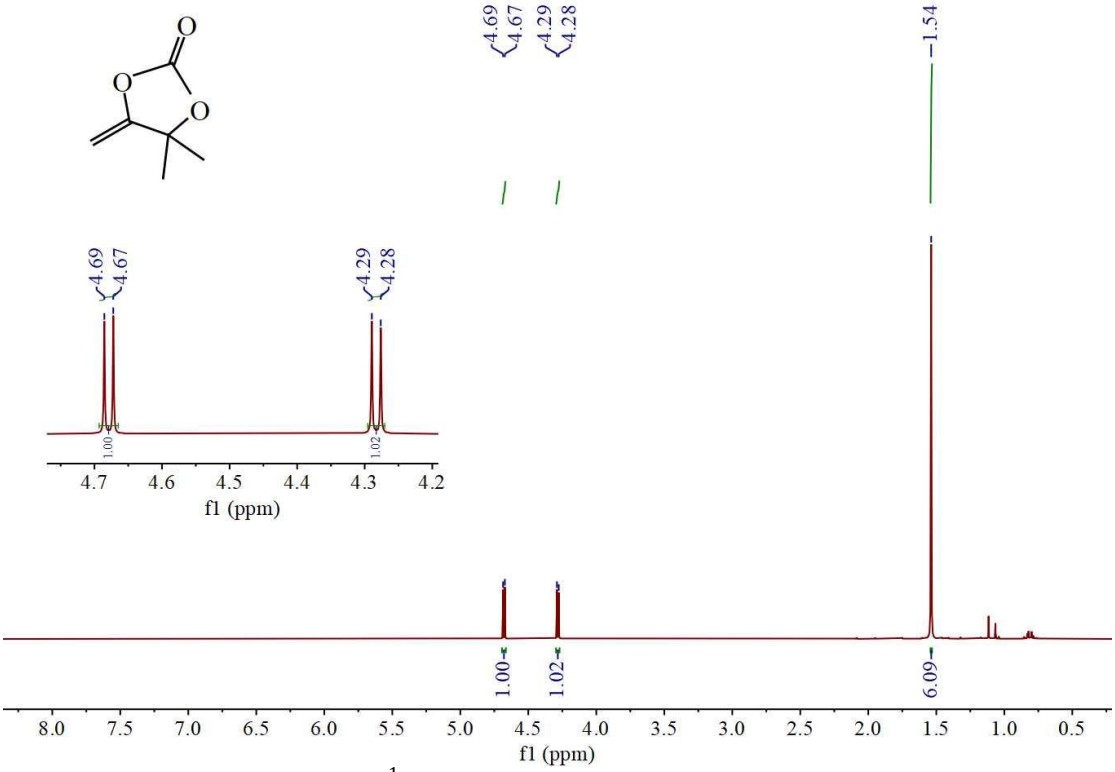


$^{1}$H NMR spectrum of **2a** in $CDCl_3$

## 4-ethyl-4-methyl-5-methylene-1,3-dioxolan-2-one (2b)

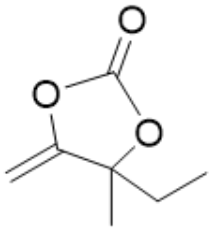

2b

$^{1}$H NMR (300 MHz, $CDCl_3$) δ = 4.77 (d, *J* = 3.9 Hz, 1H), 4.25 (d, *J* = 3.9 Hz, 1H), 1.95 – 1.80 (dq, J = 14.6 Hz, 7.4 Hz, 1H), 1.73 (dq, *J* = 14.7, 7.4 Hz, 1H), 1.55 (s, 3H), 0.94 (t, *J* = 7.4 Hz, 3H).
$^{13}$C NMR (76 MHz, $CDCl_3$) δ = 157.43, 151.61, 87.68, 85.64, 40.88, 33.39, 7.34.
The spectroscopic data matched those reported in the literature.[1]

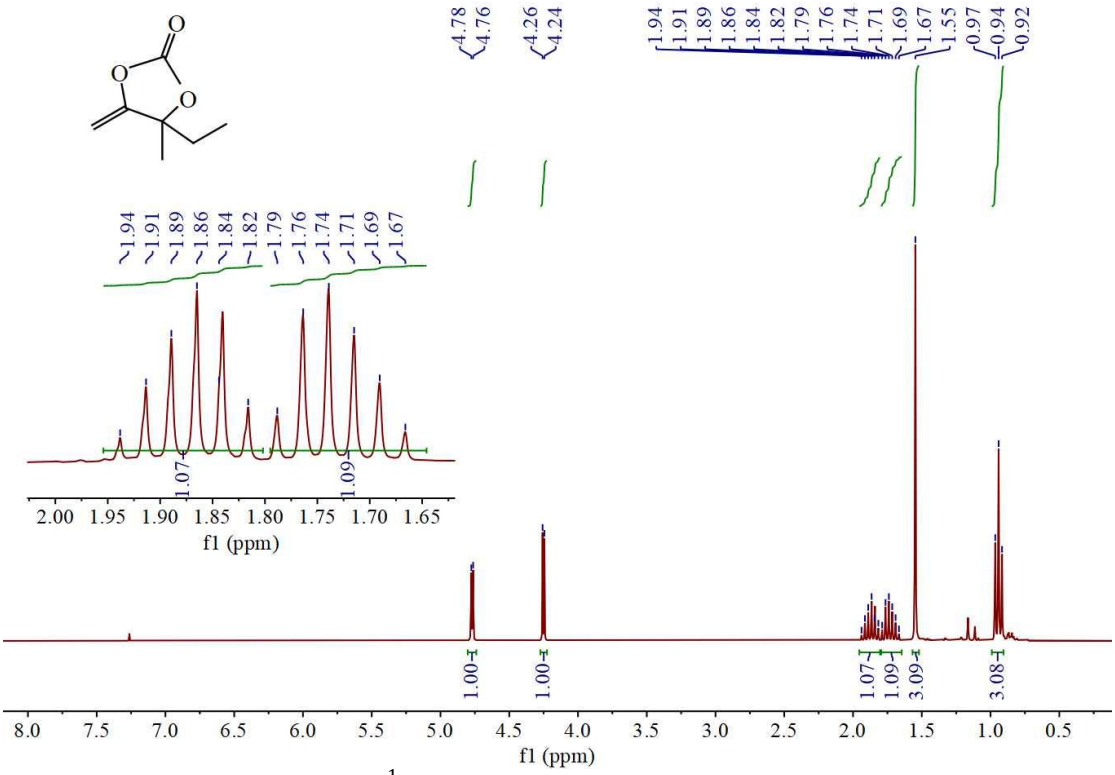


$^{1}$H NMR spectrum of **2b** in $CDCl_3$

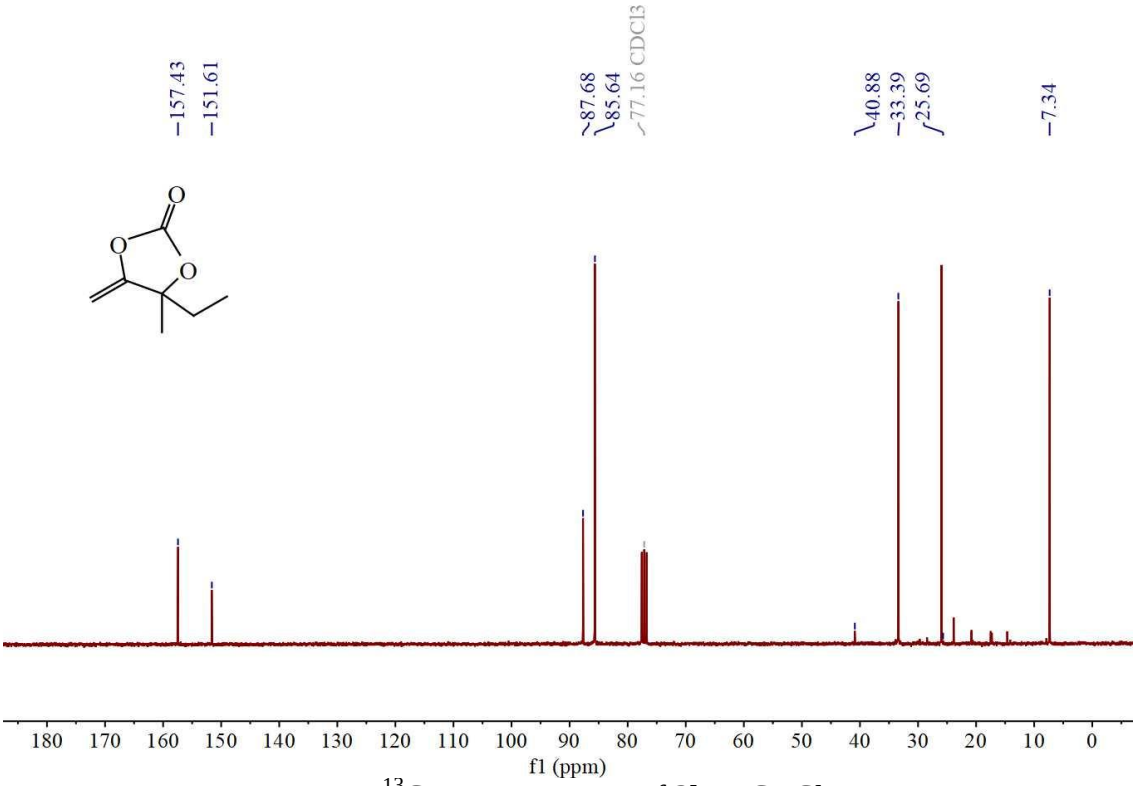


$^{13}$C NMR spectrum of **2b** in $CDCl_3$

**4,4-diethyl-5-methylene-1,3-dioxolan-2-one (2c)**

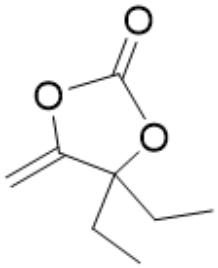

**2c**

$^{1}$H NMR (300 MHz, $CDCl_3$) δ = 4.72 (d, *J* = 3.9 Hz, 1H), 4.17 (d, *J* = 3.9 Hz, 1H), 1.81 (dq, *J* = 14.6, 7.3 Hz, 2H), 1.62 (dq, *J* = 14.7, 7.4 Hz, 2H), 0.84 (t, *J* = 7.4 Hz, 6H).
$^{13}$C NMR (76 MHz, $CDCl_3$) δ = 155.58, 151.70, 90.82, 85.77, 31.70, 6.99.

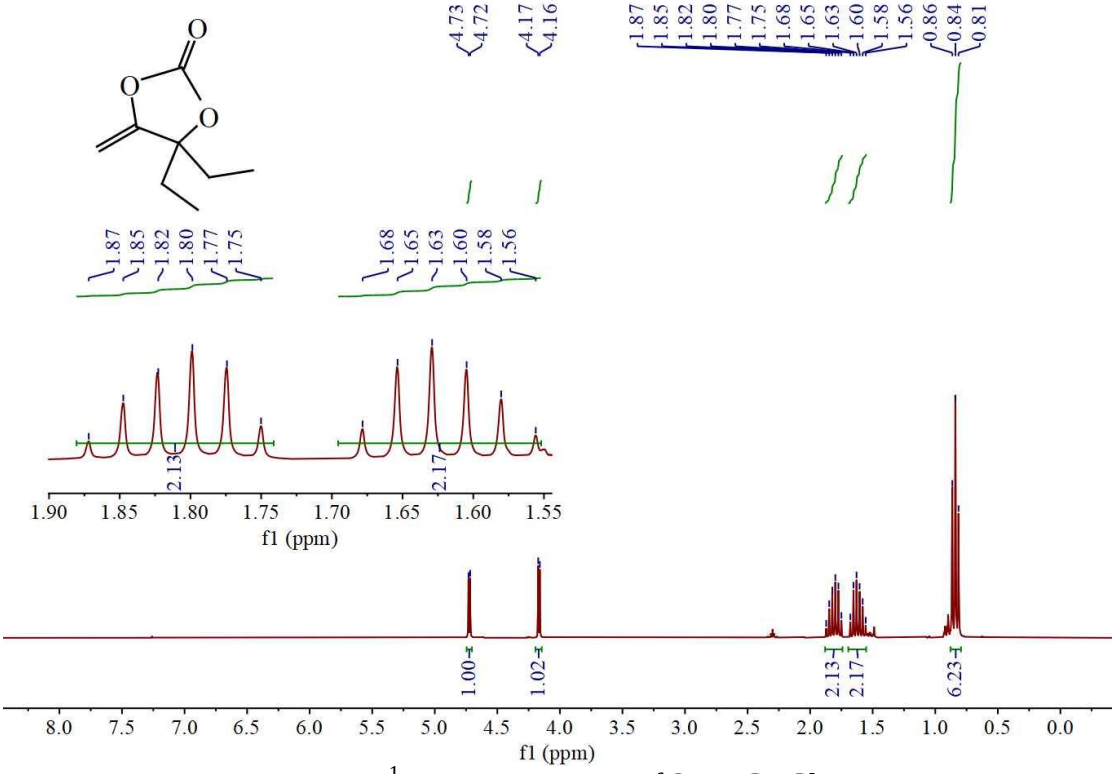


$^{1}$H NMR spectrum of **2c** in $CDCl_3$

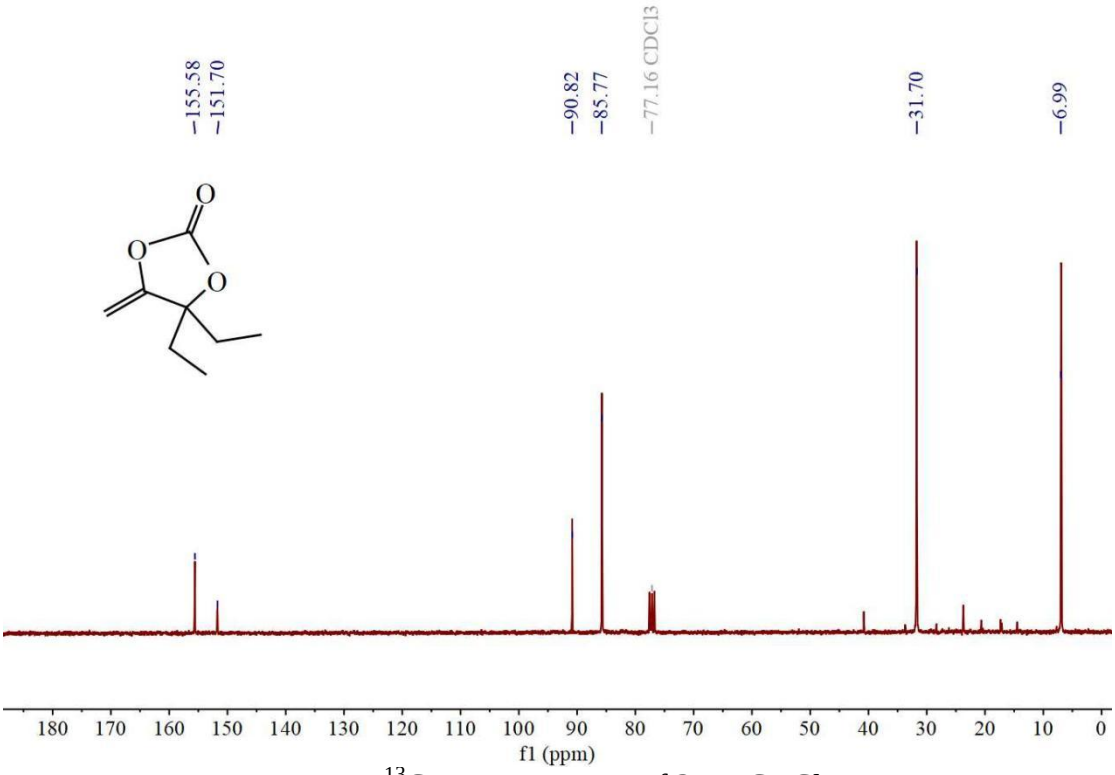


$^{13}$C NMR spectrum of **2c** in $CDCl_3$

**4-isobutyl-4-methyl-5-methylene-1,3-dioxolan-2-one (2d)**

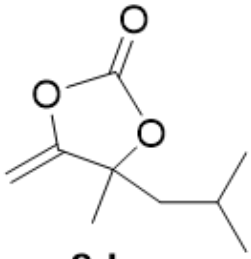

**2d**

$^{1}$H NMR (300 MHz, $CDCl_3$) δ = 4.68 (d, *J* = 3.9 Hz, 1H), 4.23 (d, *J* = 1.8 Hz, 1H), 1.90 – 1.67 (m, 2H), 1.61 (d, *J* = 8.2 Hz, 1H), 1.50 (s, 3H), 0.88 (dd, *J* = 8.1, 3.5 Hz, 6H).
$^{13}$C NMR (76 MHz, $CDCl_3$) δ = 158.20, 151.32, 87.34, 85.53, 48.35, 26.94, 24.25, 23.85, 23.57.
The spectroscopic data matched those reported in the literature.

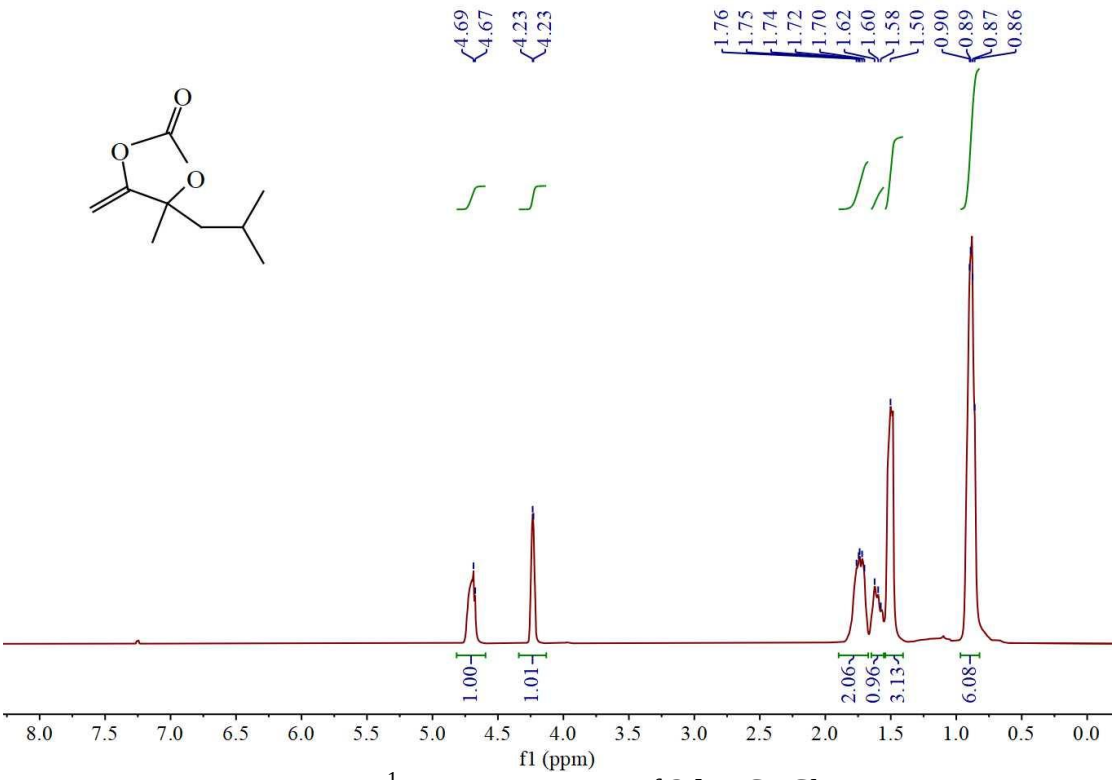


$^{1}$H NMR spectrum of **2d** in $CDCl_3$

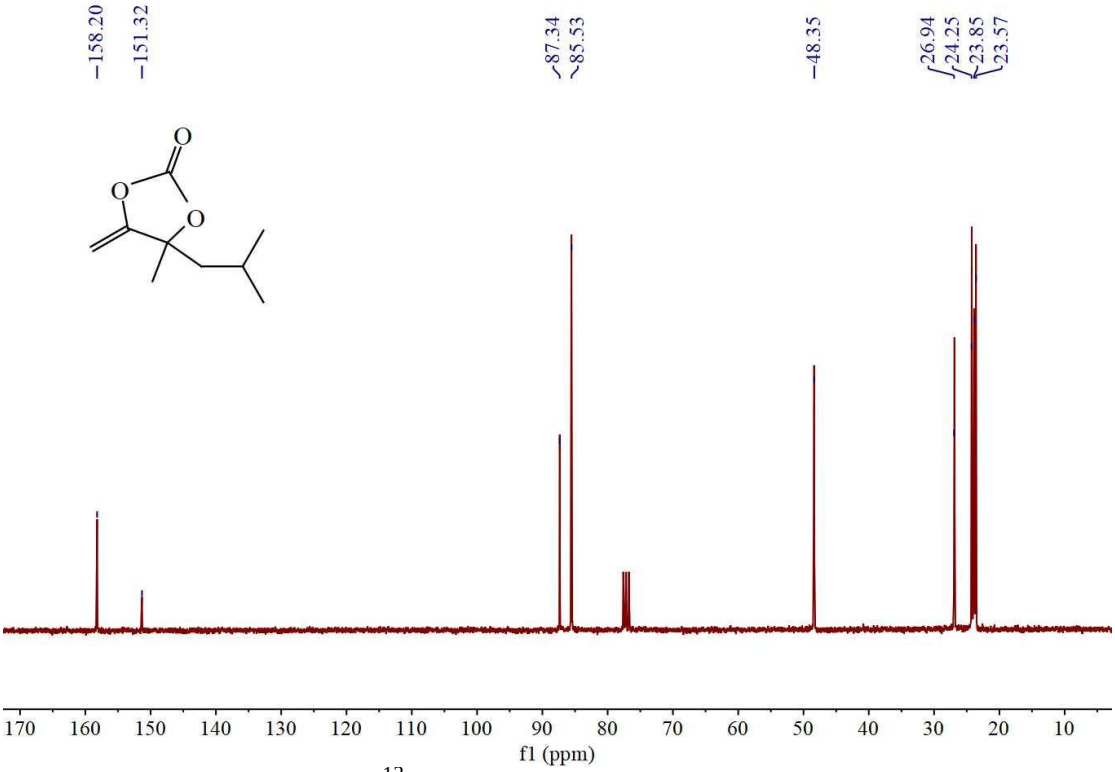


$^{13}$C NMR spectrum of **2d** in $CDCl_3$

**4-methyl-5-methylene-4-phenyl-1,3-dioxolan-2-one (2e)**

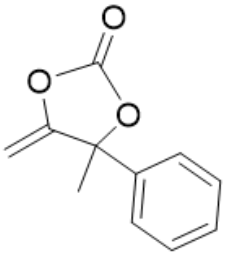

**2e**

$^{1}$H NMR (300 MHz, DMSO) δ = 7.57 – 7.51 (m, 2H), 7.50 – 7.41 (m, 3H), 4.99 (d, *J* = 4.1 Hz, 1H), 4.81 (d, *J* = 4.1 Hz, 1H), 2.00 (s, 3H).
$^{13}$C NMR (76 MHz, $CDCl_3$) δ = 157.09, 150.91, 139.10, 128.90, 128.67, 124.47, 87.95, 86.94, 26.93.
The spectroscopic data matched those reported in the literature.

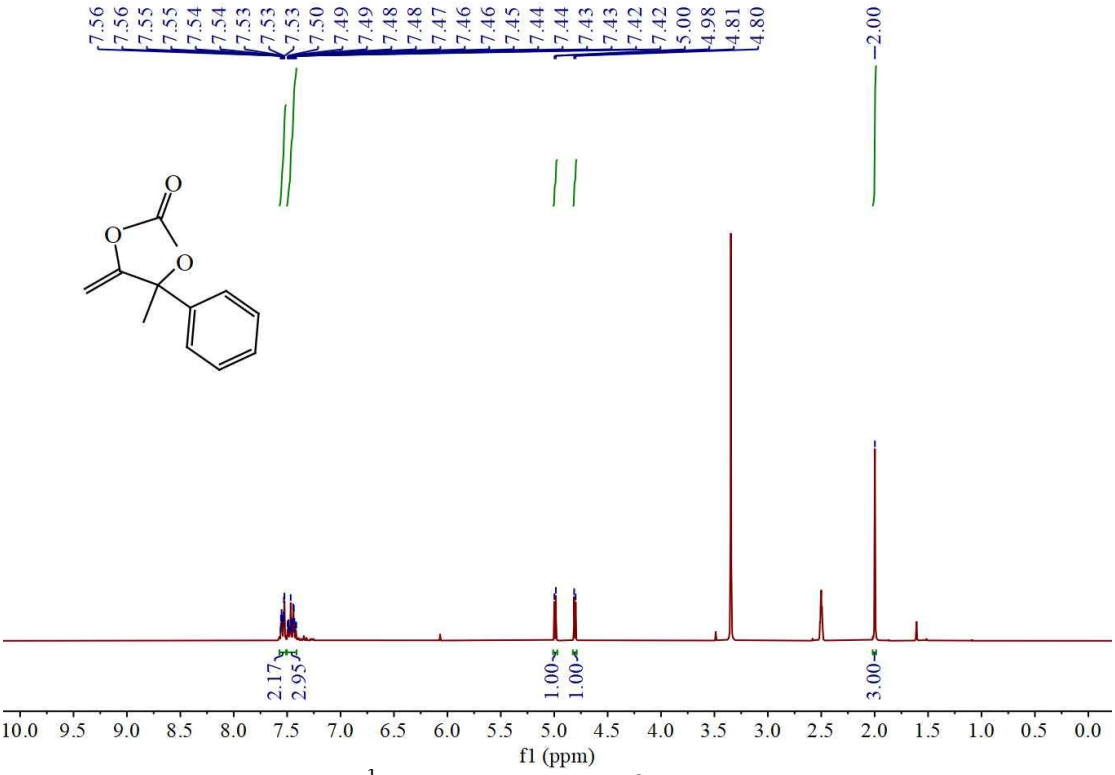


$^{1}$H NMR spectrum of **2e** in DMSO-$d_6$

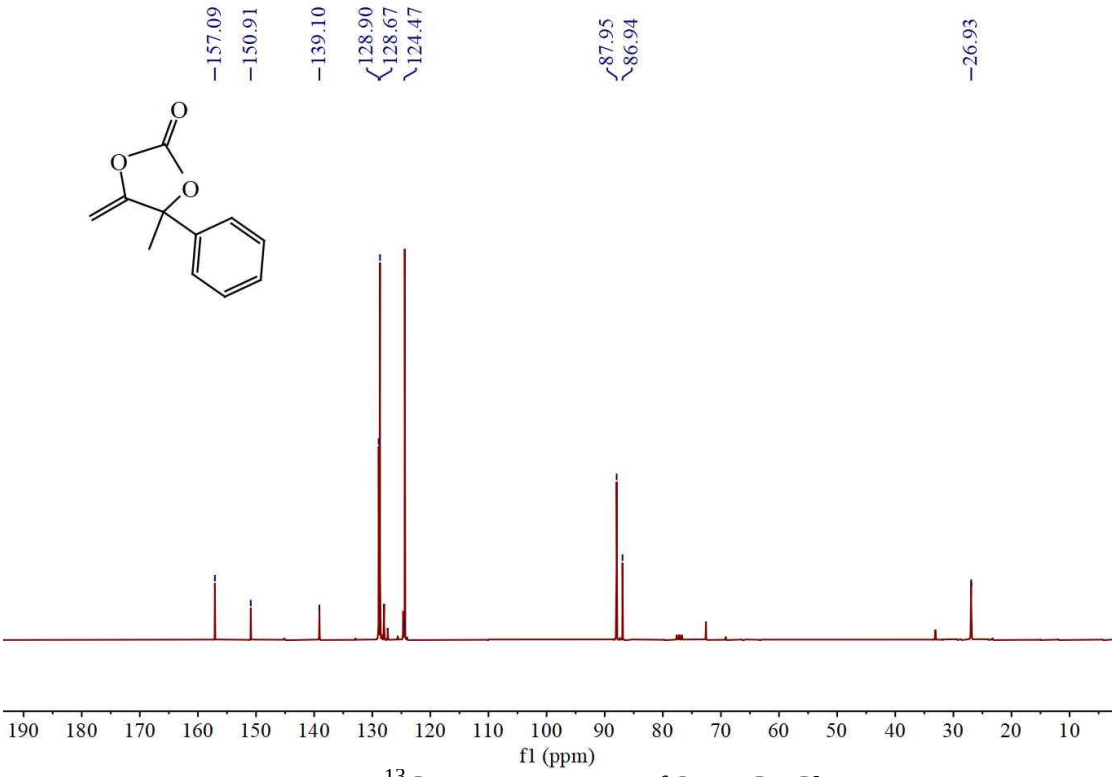


$^{13}$C NMR spectrum of **2e** in $CDCl_3$